Incorporation model of N into GaInNAs alloys grown by radio-frequency plasma-assisted molecular beam epitaxy

A. Aho, V.-M. Korpijärvi, A. Tukiainen, J. Puustinen, and M. Guina
Optoelectronics Research Centre, Tampere University of Technology, Korkeakoulunkatu 3, FI-33720 Tampere, Finland

(Received 19 September 2014; accepted 22 November 2014; published online 3 December 2014)

We present a Maxwell-Boltzmann electron energy distribution based model for the incorporation rate of nitrogen into GaInNAs grown by molecular beam epitaxy (MBE) using a radio frequency plasma source. Nitrogen concentration is predicted as a function of radio-frequency system primary resistance, N flow, and RF power, and group III growth rate. The semi-empirical model is shown to be repeatable with a maximum error of 6%. The model was validated for two different MBE systems by growing GaInNAs on GaAs(100) with variable nitrogen composition of 0%–6%.
 [http://dx.doi.org/10.1063/1.4903318]

I. INTRODUCTION

Plasma-assisted molecular beam epitaxy (PAMBE) is an attractive technique for growing III-N-V alloys[1] and has been used for demonstrating a wide range of heterostructures. In particular, the MBE growth has led to state-of-the-art demonstrations of GaInNAs(Sb)-based lasers[2,3] and 1 eV GaInNAs(Sb) solar cells.[4,5] However, the N incorporation processes using radio-frequency (RF) N plasma source requires a thorough optimization of the growth conditions and understanding of the N incorporation processes.[1,5] First of all, the growth parameters and plasma settings do not translate to a simple linear relation for the incorporation rate of N. Also, the N-ions generated by the plasma source can easily lead to poor epitaxial quality of the semiconductor wafer,[6–8] which leads to a dependence of the epitaxial quality on the selected N flow and RF power,[9–11] largely due to variations of the N ion fluxes and energies.[12] By optimizing the plasma parameters for a given N composition, the effect of the N-ions can be minimized. Thus, a useful model predicting the N composition as a function of plasma parameters could result in significantly faster calibration and optimization of GaInNAs growth. The predictive model could also be used for growth of complicated structures with different N compositions in the same growth run. So far, some incorporation models for MBE have been presented,[13–15] but they are not practical on a daily basis, since they do not predict the dissociation efficiency of N as a function of the RF power (P_{RF}). In this paper, we introduce a Maxwell-Boltzmann electron energy distribution based rate equation predicting the N composition as a function of PAMBE parameters, namely, the N flow and RF power, and group III growth rate.

II. THEORY AND MODEL

In an RF plasma source, the N_2 molecules are bombarded with RF powered electrons; the RF oscillation mainly energizes the electrons and leaves the ions unperturbed due to a large mass to charge ratio. The electron oscillation intensity is increased when the RF power is increased leading eventually to excitation, dissociation, and ionization of N species.[16] RF plasma activated N incorporates to the crystal mainly in the form of atomic N,[17] but also the other plasma activated N species contribute to the growth.[6] In general, the N RF plasma consists of electrons and the following N species (ordered descending in terms of their amount): neutral molecules (N_2), excited molecule radicals, neutral atoms, molecular ions, and atomic ions, with formation energies ~6–8, 9.7, 15.8, and 14.5 eV, respectively.[6] To establish a model for the incorporation of N, we first need to estimate the electron energy distribution and the average energy of the electrons in nitrogen plasma. The electrons are approximated to be nearly free and to move in a loop trajectory confined into a symmetric volume V_L with a loop cross-section area A_L and a loop length L_L. The plasma electrons are confined by a time variable magnetic field induced by a solenoid coil of the plasma source and the strength of the field is dependent on the intensity of the transmitted RF power (P_p). The average free electron energy E_e can be expressed as

$$E_e = \frac{E_{RF-plasma}}{n_e V_L} = kT_e, \tag{1}$$

where n_e is the free electron density, $E_{RF\text{-}plasma}$ is the time-averaged total transmitted RF energy, T_e is the average electron temperature, and k is the Boltzmann constant. If we assume the plasma loop as a conductor, where the electrons carry the current with mobility μ_e, we can estimate n_e from the plasma resistance

$$R_p = \frac{1}{e n_e \mu_e} \frac{L_L}{A_L}. \tag{2}$$

When n_e is solved from Eq. (2) and inserted to Eq. (1), we obtain

$$E_e = \frac{E_{RFtot}}{\frac{1}{R_p e \mu_e}\frac{L_L}{A_L} V_L} = \frac{2R_p \int_0^{T/2} P_p(t)dt}{\frac{1}{e\mu_e}\frac{L_L}{A_L} V_L} = \frac{2R_p P_p \int_0^{T/2} dt}{\frac{1}{e\mu_e}\frac{L_L}{A_L} V_L} = \frac{R_p P_p}{\frac{1}{e\mu_e} C(P_p, T)}, \tag{3}$$

where we define $C(P_p, T)$ as an effective electron confinement factor dependent on P_p and RF oscillation period (T). In the case of low pressure plasma, a collisionless plasma approximation can be used and therefore the energy distribution of electrons is assumed to follow a Maxwell-Boltzmann distribution, otherwise electrons follow a Druyvesteyn distribution.[16,18] In our case, the pressure of the plasma system is low and therefore it is justified to use Maxwell-Boltzmann distribution for the modelling.[16] The dissociation rate R_d of the molecules becomes[16]

$$R_d = N_m \delta(T_e) \left(\frac{8kT_e}{\pi m_e}\right)^{1/2} e^{\frac{-Ead}{kT_e}}. \tag{4}$$

Then by using Eq. (3), we get

$$\begin{aligned} R_d &= N_m \delta(T_e) \left(\frac{8e\mu_e R_p P_p}{\pi m_e C(P_p)}\right)^{1/2} \exp\left(\frac{-E_{ad} C(P_p, T)}{\mu_e R_p P_p}\right) \\ &= N_m \delta(T_e) \left(\frac{8e\mu_e}{\pi m_e C(P_p, T)}\right)^{1/2} (R_p P_p)^{1/2} \\ &\quad \times \exp\left(\frac{-E_{ad} C(P_p, T)}{e\mu_e R_p P_p}\right), \end{aligned} \tag{5}$$

where δ is the absorption cross section for inelastic electron collision processes in N_2, N_m is the density of nitrogen molecules, and E_{ad} is the activation energy for N_2 dissociation.[16] N_m can be solved from the ideal gas law

$$p_{eq} V = N_m k T_{N2} \tag{6}$$

and the Knudsen equation[19]

$$\frac{dN_{N_2}}{dt} = A(p_{eq} - p)\sqrt{\frac{N_a}{2\pi M_{N_2} k T_{N_2}}} \overset{Eq.(6)}{\approx} \frac{A N_m k T_{N_2}}{V}\sqrt{\frac{N_a}{2\pi M_{N_2} k T_{N_2}}}, \tag{7}$$

where V is the plasma source volume, p_{eq} is the plasma chamber equilibrium pressure, p is MBE system pressure, and A is the plasma source aperture area; here, we assume that

$$p_{eq} - p \approx p_{eq}. V = n \times V_m, \tag{8}$$

where n is the concentration of N_2 molecules in moles and V_m is the molar volume (22.4 l/mol). By differentiating Eq. (8) with respect to time, a relation between the molecular flows F(sccm) and $\frac{dN_2}{dt}$ (1/s) is found

$$\frac{dV}{dt} = V_m \frac{dn}{dt} = \frac{V_m}{N_a}\frac{dN_{N_2}}{dt} = \frac{1}{60s/\text{min}} F \tag{9}$$

resulting in

$$\frac{dN_{N_2}}{dt} = \frac{F \times N_a}{60s/\text{min} \times V_m}, \tag{10}$$

where N_a is the Avogadro constant. Next, we combine Eqs. (7) and (10) yielding

$$N_m = \frac{F(sccm) \times N_a \times V}{60s/\text{min} \times A \times V_m k T_{N_2} \sqrt{\frac{N_a}{2\pi M_{N_2} k T_{N_2}}}}. \tag{11}$$

From Eqs. (5) and (11), we obtain

$$\begin{aligned} R_d = &\frac{F\delta(T_e) \times V}{60s/\text{min} \times A \times V_m \times \sqrt{\frac{kT_m}{2\pi M_{N_2} N_A}}} \\ &\times \left(\frac{8e\mu_e}{\pi m_e C}\right)^{1/2} (R_p P_P)^{1/2} \exp\left(\frac{-EadC}{e\mu_e R_p P_P}\right). \end{aligned} \tag{12}$$

Next, we need to link the R_p and P_p to the system primary resistance (R_{sp}) and P_{RF}. The changes in the R_p as a function of P_{RF} and F can be estimated from the primary circuit, and the changes in the system primary resistance are directly related to the power transferred to the plasma.[20] Here, we use the plasma transformer formalism for the estimation of R_p.[21] In this model, the primary coil has n turns and the plasma itself can be modeled as a single turn coil. In an ideal transformer, where the plasma loop is modeled with a single loop coil, R_p is seen on the primary circuit as a transformed resistance[21]

$$R_{pt} = n^2 R_p. \tag{13}$$

We therefore get

$$R_{sp} = R_c + n^2 R_p, \tag{14}$$

where R_c is the resistance that simulates the RF matcher and system losses. P_p can be also estimated from the system resistances with the relation[22]

$$P_p = \frac{n^2 R_p}{R_{sp}} P_{RF} = \varepsilon P_{RF}, \tag{15}$$

where ε is the power transfer efficiency.

$$\begin{aligned} R_d \overset{Eq.15}{=} &\frac{F\delta(T_e) \times V}{60s/\text{min} \times A \times V_m \times \sqrt{\frac{kT_m}{2\pi M_{N_2} N_A}}} \left(\frac{8e\mu_e}{\pi m_e C}\right)^{1/2} \\ &\times \left(\frac{\varepsilon^2 R_{sp}}{n^2} P_{RF}\right)^{1/2} \exp\left(\frac{-E_{ad} C}{e\mu_e \frac{\varepsilon^2 R_{sp}}{n^2} P_{RF}}\right). \end{aligned} \tag{16}$$

Nitrogen incorporation is estimated by scaling R_d with a geometrical factor G accounting for the reactor and plasma source and the nitrogen sticking coefficient $S \leq 1$. S is a function of growth temperature,[23,24] nitrogen composition,[25] and arsenic flux.[15,26] Nitrogen incorporation is also inversely proportional to the group III growth rate GR_{III}.[26] Finally, for fitting with experimental data, Eq. (16) is simplified with parameters B and D, which are dependent on P_{RF} and F. Finally, we obtain an equation for the nitrogen composition

$$N(\%) = \frac{SGR_d}{GR_{III}} = \frac{B}{GR_{III}} F (R_{sp} P_{RF})^{1/2} \exp\left(\frac{-E_{ad} D}{R_{sp} P_{RF}}\right). \tag{17}$$

III. EXPERIMENTS

In order to verify the model, we grew a series of samples with two MBE systems: Veeco GEN20 and VG Semicon V80. Both systems were equipped with Veeco Sumo cells for In and Ga, cracker for As and Veeco UNI-Bulb autotuned RF (13.56 MHz) N plasma source. The plasma systems contained a commercial automatic matcher unit with L-topology. The matcher units are used for the compensation of plasma and coil reactance ensuring maximum power transfer from the RF power source to the plasma.

The GEN20 samples consisted of 200 nm thick GaInNAs layers, which were grown on n-GaAs(100) wafers. Before the epitaxial growth of GaInNAs, desorption of the native oxides was performed at 620 °C followed by growth of a GaAs buffer at 580 °C. The growth rate was 0.75 μm/h, the beam equivalent pressure ratio of As and group III atoms was 10, and the growth temperature setpoint was 440 °C. The indium composition was calibrated to 8% by separately grown GaInAs/GaAs superlattice samples. After calibration of the In composition, multiple samples were grown with different N fluxes. The active N flux was varied by changing both P_{RF} and F. The P_{RF} was varied between 150 and 350 W, while F was varied from 0.15 to 0.63 sccm. The N plasma system primary resistance was estimated from the RF power-voltage data with different powers and fluxes collected from the GEN20 reactor.

The samples grown at the V80 MBE system were 3-period GaAs/GaNAs superlattice structures composed of 20 nm GaNAs and 50 nm GaAs layers. The superlattices were grown on semi-insulating or n-doped GaAs(100). The growth rate was 0.5 μm/h and the growth temperature setpoint was 475 °C for the superlattice region. F was varied from 0.05 to 0.25 sccm and P_{RF} from 250 to 450 W. All the samples were grown in a short period of time to minimize fluctuations in the growth parameters.

X-Ray diffraction (XRD) spectra from (004) planes for both sets of samples were measured with either Philips' triple-axis or BEDE's double crystal x-ray diffractometers. The N compositions were obtained by fitting the measured XRD data to rocking curves simulated by the BEDE RADS software using dynamical diffraction theory. The N composition values were fitted to Eq. (17)[27] using the Levenberg-Marquardt algorithm. After the fitting, the model was tested by growing three GaInNAs quantum well samples (QW) with a nitrogen concentration of 1.2% with the GEN20 reactor, while varying the plasma parameters to following values: 150 W and 0.45 sccm; 227 W and 0.17 sccm; 304 W and 0.15 sccm. The quality of QW samples and corresponding emission wavelengths were compared by photoluminescence (PL) measurements. A second test with the GEN20 reactor was made for lattice matched bulk samples with 0%–6% N composition. In these samples, the In composition was tuned to 2.7 times the N composition ensuring lattice matching to GaAs.

IV. RESULTS AND DISCUSSION

First the measured RF power-voltage-data for the GEN20 reactor was analyzed; the data are summarized in Fig. 1(a). The calculated primary resistances for different F values are presented in Fig. 1(b). Primary resistance was found to be a function of F and nearly independent of the P_{RF}. Therefore, for the incorporation model, a linear interpolation for plasma resistance as a function of F was used as shown in Fig. 1(b).

The nearly monotonic decrease of plasma system resistance with F could be explained by the fact that every new nitrogen molecule inserted to the system can free more electrons to the plasma. Eventually, we expect that the resistance would start to rise as a reduction of the electron mobility in the plasma at higher flows.

The measured N compositions for the samples grown with two MBE systems and the corresponding fitted curves are presented in Fig. 2. The curves follow the N incorporation rate reported elsewhere.[13,14,17] The incorporation shows a linear growth at low F values followed by a saturation region at high F. The fitted dependence also predicts that the incorporation rate should start to decrease for the high flows. This is actually seen for the samples grown with 150 W RF power on Gen20 reactor. With our plasma systems, the descending sides were not studied thoroughly due to plasma instability in this parameter range, which often leads to unwanted plasma shut-off. However, the decrease of the

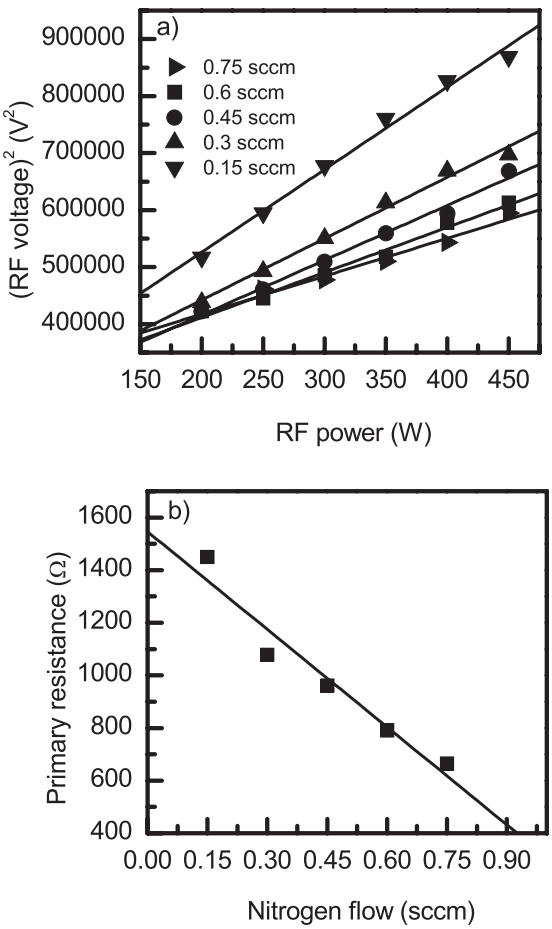

FIG. 1. (a) Square of the RF plasma voltage as a function of the plasma RF power. The linear behavior indicates that the plasma primary resistance remains constant as a function of P_{RF}, but depends on the nitrogen flow. (b) Primary resistance as a function of N_2-flow.

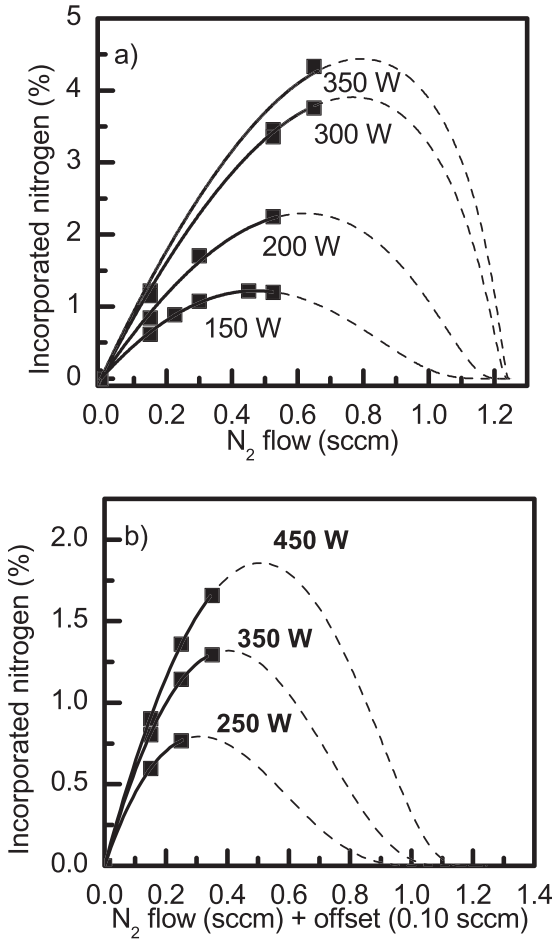

FIG. 2. Measured nitrogen compositions and the fitted curves predicted by the model for GEN20 (a) and V80 (b) reactors. The results were normalized to 1 μm/h growth rate. The fitted lines are drawn as solid in the experimentally tested range and as dashed lines on the range that was not tested in this study.

incorporation rate at high flows has been reported elsewhere in connection with the growth of GaN.[17]

Using the nominal F values for the V80 reactor, the curves could not be fitted with the requirement that they start from zero incorporation. Therefore, a constant offset of +0.10 sccm was added to the F values for the V80 reactor. This offset could be caused by an inherent offset in the N mass flow controller. For the GEN20, no offset was used. The shape differences between the curves also arise from different N-source nozzles, R_c values, reactor geometries, and configurations. Additionally, the V80 samples comprised of GaAsN, which has been observed to deviate from Vegard's law at high N compositions (although we note that in this study all but one GaAsN sample had N composition below 3% so a clear deviation is not expected[25]). The curves in Fig. 2 have only 2.6% and 0.2% deviations from the measured values in average for GEN20 and V80 reactors, respectively.

The fitting parameters B and $E_{ad}D$ are plotted in Fig. 3 as a function of P_{RF}. $R_{sp}(F)$ for the V80 reactor was adopted from the GEN20 reactor, they were not separately measured. The fitting parameters are assumed to be independent of F. In other words, the electrons are assumed to be free and only the RF power can affect the average thermal energy of the electrons. This assumption is well supported by the measured system primary resistance. In order to clarify the power dependencies of the $B(P_{RF})$ and $E_{ad}D(P_{RF})$ parameters, we used exponential fitting functions. The functions are

$$B(P_{RF}) = a_B \exp(P_{RF} t_B) + b_B \tag{18}$$

and

$$E_{ad}D(P_{RF}) = a_d \exp(P_{RF} t_d) + b_d, \tag{19}$$

where a_B, a_d, b_B, b_d, t_B, and t_d are constants. For simplicity, we use here unity power transfer efficiency and $n = 1$ for the primary coil. Fitting parameters for the GEN20 and V80 reactors are presented in Table I and Fig. 3. The fitting parameters can be interpolated accurately by the exponential functions described above. The B-parameter for both reactors decreases monotonically as a function of power, which could be linked to changes in the absorption cross section or to a power dependent plasma chamber pressure. The shape differences between the GEN20 and V80H curves may be linked to different plasma source aperture nozzles. The power dependence of E_{ad}D could be explained by changes in the effective activation energy E_{ad} or by the fact that the plasma is tighter confined when the P_{RF} is increased. The latter is considered the most probable reason. The fitting parameters also include the effect of the RF power and the N flow on the power transfer efficiency, which can be significantly lower at low plasma powers and low flows.[20–22]

To test the accuracy of the model, we used it to predict the N composition in grown crystals. To this end, we grew three QW samples with different combinations of P_{RF} and F, yet all aimed at having the same N composition. In the same way, we forecasted the compositions of five lattice matched

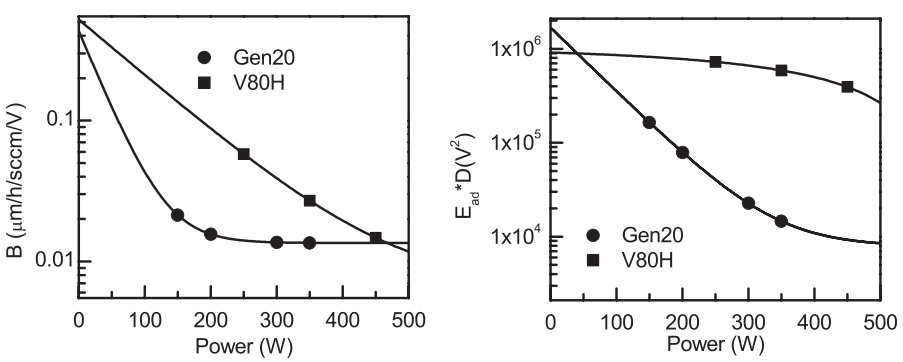

FIG. 3. Fitting parameters B and E_{ad}D as a function of the RF power.

TABLE I. Fitting parameters for the GEN20 and V80 reactors.

Reactor	a_B (μm/h/sccm/V)	t_B(1/W)	b_B (μm/h/sccm/V)	a_d (V^2)	t_d (1/W)	b_d (V^2)
GEN20	4.204×10^{-1}	-2.650×10^{-2}	1.352×10^{-2}	1.680×10^{6}	-1.578×10^{-2}	7.879×10^{3}
V80H	5.155×10^{-1}	-9.230×10^{-3}	6.640×10^{-3}	-1.280×10^{5}	3.610×10^{-3}	1.042×10^{6}

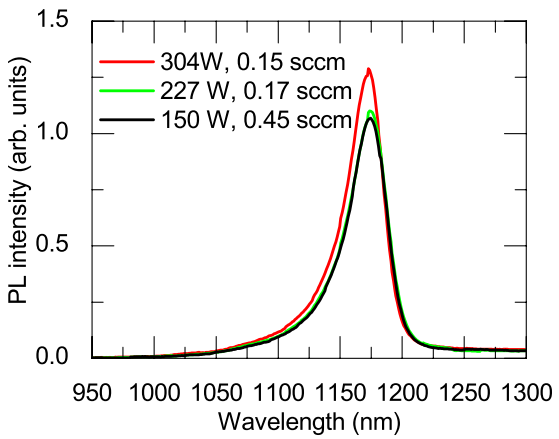

FIG. 4. PL from GaInNAs QW samples grown with different plasma parameters aimed at the same N composition.

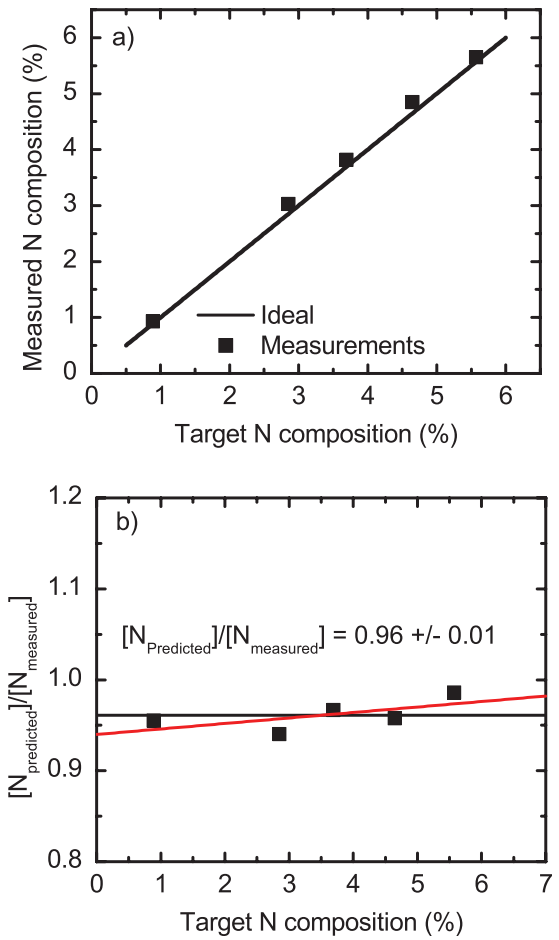

FIG. 5. (a) Comparison of predicted and measured N composition for the GaInNAs bulk samples. (b) Division of the target and measured composition. Results show that the model has 4% average error with 6% maximum error.

bulk samples with N composition form 1%–6% grown with different plasma parameters. The results are presented in Fig. 4, in which we can see that the QWs emit at precisely the same emission wavelength. This is a clear indication that all samples have same N composition despite the fact that various combinations of plasma power and flow were used. The slight differences in the peak intensities can be explained by the differences in the ratio of atomic N and N-ions produced.

For the bulk layers, the targeted N composition corresponds very well to the values from XRD simulations, as revealed in Fig. 5. The values seem to have a small calibration related drift, which becomes smaller when the N composition is increased. Nevertheless, all the samples have a maximum deviation of 6% from the model, and the average deviation is only 4%. The error is mainly systematic and can be easily corrected. After the correction, the prediction would deviate only approximately 1% from the measured values. This means that the N incorporation can be estimated with the same precision as the group III fluxes can be determined from ion gauge measurements. Furthermore, the model has been used on a daily basis at the GEN20 reactor for numerous samples; it has proved to be a helpful tool for complex GaInNAsSb solar cell and laser epitaxy.

V. CONCLUSION

We have derived a Maxwell-Boltzmann electron energy distribution based equation for the incorporation rate of N from a plasma source as a function of RF power, N flow, and group III growth rate. The model was tested for GaInNAs samples grown using Veeco GEN20 and VG Semicon V80H reactors with Veeco UNI-bulb nitrogen RF plasma sources. For both reactors, the model can be used with an absolute deviation better than 6%. The model has also been reliable in the long term use and has proved to be a versatile tool for dilute nitride epitaxy. The model and the same calibration sequence should be applicable to other nitride based PAMBE systems and RF plasma sources.

ACKNOWLEDGMENTS

The authors would like to thank colleagues at Optoelectronics Research Centre for their high-quality experimental support. For the financial support, we would like to thank Finnish Funding Agency for Technology and Innovation—TEKES (Project Nos. #40120/09 “Solar III–V” and #40239/12 “Nextsolar”), Graduate School in Electronics, Telecommunications and Automation, Ulla Tuominen Foundation, Finnish Foundation for Technology Promotion, and Wärtsilä Foundation.

[1]M. Guina and S. M. Wang, "Chapter 9—MBE of dilute-nitride optoelectronic devices," in *Molecular Beam Epitaxy*, edited by M. Henini (Elsevier, Oxford, 2013), pp. 171-187.
[2]J. Konttinen and V.-M. Korpijärvi, Nanoscale Res. Lett. **9**, 82 (2014).
[3]M. Guina, T. Leinonen, A. Härkönen, and M. Pessa, New J. Phys. **11**, 125019 (2009).
[4]M. Wiemer, V. Sabnis, and H. Yuen, "High and low concentrator systems for solar electric applications VI," Proc. SPIE **8108**, 810804 (2011).
[5]A. Aho, V. Polojärvi, V.-M. Korpijärvi, J. Salmi, A. Tukiainen, P. Laukkanen, and M. Guina, Sol. Energy Mater. Sol. Cells **124**, 150–158 (2014).
[6]N. Newman, J. Cryst. Growth **178**, 102–112 (1997).
[7]M. M. Oye, T. J. Mattord, G. A. Hallock, S. R. Bank, M. A. Wistey, J. M. Reifsnider, A. J. Ptak, H. B. Yuen, J. S. Harris, Jr., and A. L. Holmes, Appl. Phys. Lett. **91**, 191903 (2007).
[8]J. Miguel-Sánchez, A. Guzmán, and E. Muñoz, Appl. Phys. Lett. **85**, 1940 (2004).
[9]D. J. Economou, D. R. Evans, and R. C. Alkire, J. Electrochem. Soc. **135**(3), 756 (1988).
[10]T. Kageyama, T. Miyamoto, S. Makino, F. Koyama, and K. Iga, J. Cryst. Growth **209**, 350–354 (2000).
[11]M. A. Wistey, S. R. Bank, H. B. Yuen, H. Bae, and J. S. Harris, Jr., J. Cryst. Growth **278**, 229–233 (2005).
[12]J. M. Reifsnider, S. Govindaraju, and A. L. Holmes, Jr., J. Cryst. Growth **243**, 396–403 (2002).
[13]H. Carrere, A. Arnoult, A. Ricard, and E. Bedel-Pereira, J. Cryst. Growth **243**, 295–301 (2002).
[14]D. Voulot, R. W. McCullough, W. R. Thompson, D. Burns, J. Geddes, G. J. Cosimini, E. Nelson, P. P. Chow, and J. Klaassen, J. Cryst. Growth **201**/**202**, 399–401 (1999).
[15]V. A. Obnoblyudov, A. R. Kovsh, A. E. Zhukov, N. A. Maleev, E. S. Semenova, and V. M. Ustinov, Semiconductors **35**(5), 533–538 (2001).
[16]J. A. Thornton, Thin Solid Films **107**, 3–19 (1983).
[17]J. Osaka, M. Senthil Kumar, H. Toyoda, T. Ishijima, H. Sugai, and T. Mizutani, Appl. Phys. Lett. **90**, 172114 (2007).
[18]M. Druyvesteyn and F. Penning, Rev. Mod. Phys. **12**(2), 87–174 (1940).
[19]M. A. Herman and H. Sitter, *Molecular Beam Epitaxy, Fundamentals and Current Status*, 2 ed. (Springer, 1996).
[20]V. A. Godyak, R. B. Piejak, and B. M. Alexandrovich, Plasma Sources Sci. Technol. **3**, 169 (1994).
[21]R. B. Piejak, V. A. Godyak, and B. M. Alexandrovich, Plasma Sources Sci. Technol. **1**, 179–186 (1992).
[22]V. A. Godyak, R. B. Piejak, and B. M. Alexandrovich, J. Appl. Phys. **85**, 703 (1999).
[23]Z. Pan, L. H. Li, W. Zhang, Y. W. Lin, and R. H. Wu, Appl. Phys. Lett. **77**, 214 (2000).
[24]V.-M. Korpijärvi, A. Aho, P. Laukkanen, A. Tukiainen, A. Laakso, M. Tuominen, and M. Guina, J. Appl. Phys. **112**, 023504 (2012).
[25]W. Li, M. Pessa, and J. Likonen, Appl. Phys. Lett. **78**(19), 2864 (2001).
[26]G. Jaschke, R. Averbeck, L. Geelhaar, and H. Riechert, J. Cryst. Growth **278**, 224–228 (2005).
[27]Origin 8.0, OriginLab, Northampton, MA.